PHYSICAL REVIEW B **78**, 180507(R) (2008)

Transverse commensurability effect for vortices in periodic pinning arrays

C. Reichhardt and C. J. Olson Reichhardt
Theoretical Division, Los Alamos National Laboratory, Los Alamos, New Mexico 87545, USA
(Received 11 August 2008; revised manuscript received 21 October 2008; published 24 November 2008)

Using computer simulations, we demonstrate a type of commensurability that occurs for vortices moving longitudinally through periodic pinning arrays in the presence of an additional transverse driving force. As a function of vortex density, there is a series of broad maxima in the transverse critical depinning force that do not fall at the matching fields where the number of vortices equals an integer multiple of the number of pinning sites. The commensurability effects are associated with dynamical states in which evenly spaced structures consisting of one or more moving rows of vortices form between rows of pinning sites. Remarkably, the critical transverse depinning force can be more than an order of magnitude larger than the longitudinal depinning force.

DOI: 10.1103/PhysRevB.78.180507 PACS number(s): 74.25.Qt

Matching effects for vortices in periodic pinning arrays have been studied extensively for different types of pinning lattice geometries.[1–6] As a function of magnetic field, the critical current passes through a series of peaks generated by commensurability effects that occur when the number of vortices equals an integer multiple of the number of pinning sites and the vortex ground state is an ordered crystalline structure.[2–4] When each pinning site can capture only one vortex, the excess vortices at fields above the first matching field are located in interstitial sites and depin first under an external drive.[2–4,6,7] Once the interstitial vortices are moving under a longitudinal drive, it is possible to apply an additional transverse drive in the direction perpendicular to the vortex motion. In this case, although the vortices are mobile in the longitudinal direction, they can remain pinned in the transverse direction and there can be a finite transverse critical depinning threshold.

The possibility of a transverse depinning threshold for moving vortices was initially predicted for systems with random pinning when the moving vortices form well-defined channels,[8] and transverse depinning thresholds in randomly pinned systems have been observed in numerical simulations[9] and experiments.[10,11] For vortices moving in the presence of a periodic pinning array, a finite transverse depinning threshold has been measured at high drives when all of the vortices are moving and has a value that depends on the angle between the longitudinal driving direction and a symmetry axis of the pinning lattice. Here, the most prominent transverse depinning thresholds and dynamical locking effects occur for driving along the principal axes of the pinning lattice.[12,13] This type of effect has been experimentally observed for colloidal particles moving over periodic substrates.[14] When only one vortex can be captured by each pinning site, motion of the vortices at low drives occurs as a flow of interstitial vortices between vortices that remain trapped at the pinning sites.[2,3,6] In this case, it is not known whether a transverse depinning threshold exists, and in general it is not known how the transverse depinning threshold varies with magnetic field.

It might be expected that the transverse depinning threshold would simply exhibit peaks at the same magnetic fields where peaks in the longitudinal depinning threshold appear. In this Rapid Communication, we demonstrate that although there are enhancements of the transverse depinning threshold at certain fields, these fields are *not related* to fields which produce peaks in the longitudinal depinning threshold but are instead associated with *dynamical* matching conditions. The distinct dynamical matching effects appear because the moving vortices assume a different structure than the static vortex ground state. Dynamical commensurability effects occur when an integer number of moving interstitial vortex rows form between adjacent rows of pinning sites. The dynamical matching effects are much broader than the static matching effects and have maxima that encompass several static matching fields. An oscillatory critical current appears for the dynamical transverse commensurability effect. This is similar to the critical current oscillations seen for vortices depinning in artificial channels[15,16] or in layered or strip geometries,[17,18] although in the channel, layer, or strip systems, the commensurations arise due to matching effects of the vortex ground state rather than the dynamical matching effects observed in the present work. Remarkably, we find that the transverse depinning threshold can be up to an order of magnitude larger than the longitudinal depinning threshold.

We numerically simulate a two-dimensional system with periodic boundary conditions in the x and y directions containing N_v vortices and N_p pinning sites following a procedure similar to that used in previous simulations for vortices in periodic pinning arrays. The number of vortices is proportional to the applied magnetic field $\mathbf{B}=B\hat{\mathbf{z}}$, which is normal to our simulation plane. The repulsive vortex-vortex interaction force is given by $\mathbf{F}_i^{vv}=\Sigma_{i\neq j}^{N_v} f_0 K_1(R_{ij}/\lambda)\hat{\mathbf{R}}_{ij}$, where K_1 is a modified Bessel function, $R_{ij}=|\mathbf{R}_i-\mathbf{R}_j|$ is the distance between vortex i and j located at $\mathbf{R}_i$ and $\mathbf{R}_j$, $\hat{\mathbf{R}}_{ij}=(\mathbf{R}_i-\mathbf{R}_j)/R_{ij}$, $f_0=\phi_0^2/(2\pi\mu_0\lambda^3)$, $\phi=h/2e$ is the elementary flux quantum, and λ is the London penetration depth. The pinning sites are placed in a triangular lattice, and the field at which the number of pinning sites equals the number of vortices, $N_p=N_v$, is defined as the matching field B_ϕ. The individual pinning sites are modeled as parabolic traps of radius $r_p=0.35\lambda$ and strength $F^p=1.25$, with $\mathbf{F}_i^p=\Sigma_k^{N_p} F^p f_0(R_{ik}/r_p)\Theta(r_p-R_{ik})\hat{\mathbf{R}}_{ik}$, where Θ is the Heaviside step function, $R_{ik}=|\mathbf{R}_i-\mathbf{R}_k^p|$, $\hat{\mathbf{R}}_{ik}=(\mathbf{R}_i-\mathbf{R}_k^p)/R_{ij}$, and $\mathbf{R}_k^p$ is the location of pin k. The overdamped equation of motion for a vortex i is

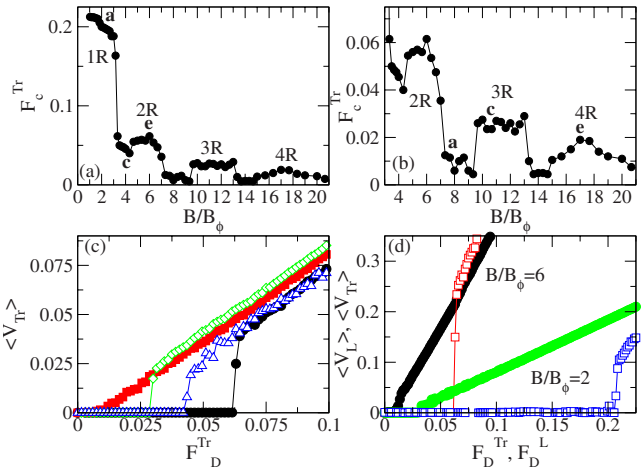

FIG. 1. (Color online) (a) The transverse critical depinning force F_c^{Tr} vs B/B_ϕ for a system with $B_\phi=0.052\phi_0/\lambda^2$ and fixed longitudinal drive $F_D^{\mathrm{L}}=0.6$. The points **a**, **c**, and **e** refer to the fields illustrated in Fig. 2. The maxima are labeled according to the number of moving vortex rows between adjacent pinning rows: 1R, one row; 2R, two rows; 3R, three rows; and 4R, four rows. (b) A blow up of panel (a) for $B/B_\phi>2.0$. The points **a**, **c**, and **e** refer to the fields illustrated in Fig. 3. (c) The transverse velocity $\langle V_{\mathrm{Tr}}\rangle$ vs transverse force F_D^{Tr} for $B/B_\phi=4.33$ (open triangles), 6.0 (filled circles), 8.0 (filled squares), and 10 (open diamonds). (d) The scaled longitudinal velocity $\langle V_{\mathrm{L}}\rangle(N_v/N_p)$ (filled circles) versus longitudinal drive F_D^{L} and transverse velocity $\langle V_{\mathrm{Tr}}\rangle(N_v/N_p)$ (open squares) vs transverse drive F_D^{Tr} for $B/B_\phi=6.0$ (left curves) and 2.0 (right curves).

$$\eta\frac{d\mathbf{R}_i}{dt}=\mathbf{F}_i^{vv}+\mathbf{F}_i^{p}+\mathbf{F}^{\mathrm{ext}}, \tag{1}$$

where $\eta=1$ is the viscous damping term. $\mathbf{F}^{\mathrm{ext}}$ represents the net force from an applied current and is given by $\mathbf{F}^{\mathrm{ext}}=F_D^{\mathrm{L}}f_0\hat{\mathbf{x}}+F_D^{\mathrm{Tr}}f_0\hat{\mathbf{y}}$, where the longitudinal drive F_D^{L} is applied in the x direction and the transverse drive F_D^{Tr} is applied in the y direction. The initial vortex positions are obtained by simulated annealing. The drive is first applied in the longitudinal direction in increments of $\Delta F_D^{\mathrm{L}}=0.0015$, with 15 000 simulation time steps spent at each current increment. Once the longitudinal drive reaches the desired value, it is held fixed while the transverse drive is increased from zero with the same current increment protocol. We find that our increment rate is sufficiently slow to avoid any transient effects. The longitudinal and transverse critical depinning thresholds, F_c^{L} and F_c^{Tr}, are obtained by measuring the vortex velocity $\langle V_\alpha\rangle=N_v^{-1}\Sigma_i^{N_v}\mathbf{v}_i\cdot\hat{\alpha}$, with $\alpha=x,y$, and identifying the driving force at which $\langle V_\alpha\rangle>0.001$.

We first study a system with a low pinning density to ensure that a portion of the vortices is located in the interstitial sites. The existence of a clearly defined depinning threshold which varies nonmonotonically with field is illustrated in Fig. 1(c), where we show $\langle V_{\mathrm{Tr}}\rangle$ versus F_D^{Tr} for $B/B_\phi=4.33$, 6.0, 8.0, and 10.0 in a system with $B_\phi=0.052\phi_0/\lambda^2$ and fixed $F_D^{\mathrm{L}}=0.6$. From a series of simulations, we obtain the variation in F_c^{Tr} versus B/B_ϕ plotted in Fig. 1(a). Four well-defined maxima in F_c^{Tr} appear that are centered near $B/B_\phi=2.0$, 6.0, 12.0, and 17.0. Figure 1(b) shows a blowup of the region $B/B_\phi>2.0$, where the oscillation in F_c^{Tr} can be seen more clearly. This oscillation is distinct from the matching effects observed for longitudinal depinning,[1,3–5] where well-defined peaks occur at integer matching fields. The maxima in Fig. 1(a) are much broader than in the longitudinal depinning case and each encompass three or more matching fields. Similarly, the minima in F_c^{Tr} also each spread over several values of B/B_ϕ.

For all fields $B/B_\phi>1.0$, we find that F_c^{Tr} is significantly larger than the longitudinal critical force F_c^{L}, as shown in Fig. 1(d) where we plot $\langle V_{\mathrm{L}}\rangle(N_v/N_p)$ versus F_D^{L} and $\langle V_{\mathrm{Tr}}\rangle(N_v/N_p)$ vs F_D^{Tr}. Here the velocities have been scaled by N_p rather than N_v for presentation purposes. For $B_\phi=2.0$, the transverse depinning threshold F_c^{Tr} is about six times higher than the longitudinal depinning threshold F_c^{L}. Both depinning thresholds are lower for $B/B_\phi=6.0$; however, F_c^{Tr} is again much higher than F_c^{L}. We note that the curves in Figs. 1(c) and 1(d) do not extrapolate back to the origin because for $F_D\ll F_p$ some vortices remain pinned and the flow is plastic.

In Fig. 2(a) we show the vortex and pinning site positions for point **a** in Fig. 1(a) at $B/B_\phi=2.67$, and in Fig. 2(b) we illustrate the vortex trajectories for $F_D^{\mathrm{Tr}}\lesssim F_c^{\mathrm{Tr}}$ just below the transverse depinning transition. There is a single row of moving interstitial vortices between neighboring rows of pinning sites and the vortex lattice is anisotropic, with higher vortex density in the interstitial rows than in the pinned rows. The same vortex structure appears for $1.0<B/B_\phi<2.9$, corresponding to the maximum in F_c^{Tr} marked 1R in Fig. 1(a). In Fig. 2(c), we plot the vortex positions for $B/B_\phi=4.0$ at a minimum of F_c^{Tr} found at the point marked **c** in Fig. 1(a). The interstitial rows are no longer uniform and consist of an interlacing of double rows with single rows. Figure 2(d) shows that the vortex trajectories at this field are more disordered. The vortex positions and trajectories at point **e** in the region marked 2R in Fig. 1(a) for $B/B_\phi=6.0$ appear in Figs. 2(e) and 2(f). Here there are two well-defined rows of moving vortices between adjacent pinning site rows.

We find that maxima in F_c^{Tr} occur whenever there is an integer number of moving rows of interstitial vortices between neighboring pinning rows. Since the number of vortices in each interstitial row can vary over a considerable range without destroying the row structure, the maxima in F_c^{Tr} are much broader than the peaks in F_c^{L} associated with longitudinal commensuration effects. The row structures become increasingly anisotropic with increasing field until a buckling transition occurs which marks the end of the maximum in F_c^{Tr}. In Fig. 3(a) we illustrate the vortex positions for $B/B_\phi=8.0$ at a minimum in F_c^{Tr} found at the point marked **a** in Fig. 1(b). The interstitial vortices form a mixture of two and three interstitial rows between pinning site rows, producing the nonuniform trajectories shown in Fig. 3(b). At the maximum in F_c^{Tr} marked **c** in Fig. 1(b), corresponding to $B/B_\phi=10.67$, Figs. 3(c) and 3(d) show that there are three well-defined rows of moving vortices between adjacent pinning site rows. Similarly, Figs. 3(e) and 3(f) indicate that there are four interstitial vortex rows at $B/B_\phi=17$, which falls on the maximum in F_c^{Tr} at the point marked **e** in Fig. 1(b). Near $B/B_\phi=14$, where F_c^{Tr} passes through a minimum, the interstitial vortices form a mixture of three and four rows,

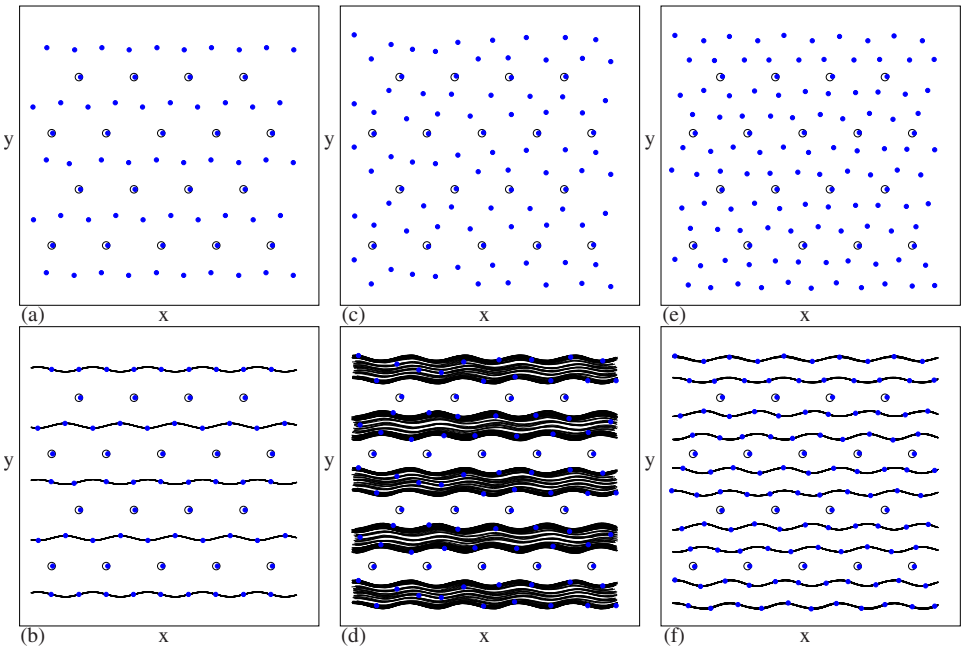

FIG. 2. (Color online) The vortex positions (black dots), pinning site locations (open circles), and vortex trajectories (black lines) for the system in Fig. 1(a). [(a),(b)] $B/B_\phi=2.67$, marked **a** in Fig. 1(a). [(c),(d)] $B/B_\phi=4.0$, marked **c** in Fig. 1(a). [(e),(f)] $B/B_\phi=6.0$, marked **e** in Fig. 1(a).

while for $B/B_\phi \gtrsim 19$ there is a mixture of four and five interstitial rows (not shown).

Commensurability effects generated by the presence of an integer number of vortex rows between linelike barriers have been observed for longitudinal vortex motion through channel geometries[15,16] as well as critical currents in layered materials,[17] superconducting strips,[18] and anisotropic pinning arrays.[19] In all these cases the commensurability occurs in the *static* vortex configurations. This is distinct from the transverse depinning maxima that we observe here, which arises due to commensurations in the *dynamical* interstitial vortex configuration. Reference 16 predicts a dependence $B \propto (n-1)^2$ of the matching field on the number n of static rows for $n \geq 2$; we expect a similar dependence for our dynamical vortex rows.

As shown in Fig. 1(c), the transverse depinning threshold is much higher than the longitudinal depinning threshold. In Fig. 4(a) we quantify this effect by plotting F_c^{L} and F_c^{Tr} as a function of pinning density B_ϕ for a commensurate field $B/B_\phi=2.0$ where F_c^{L} passes through a peak and for an incommensurate field $B/B_\phi=2.5$. At the incommensurate field, F_c^{L} and F_c^{Tr} are both reduced. At $B/B_\phi=2.0$, F_c^{L} increases monotonically with B_ϕ while F_c^{Tr} shows a smaller increase; however, F_c^{Tr} is significantly larger than F_c^{L} over the entire range of pinning densities studied. At the incommensurate field $B/B_\phi=2.5$, we find a similar trend; however, F_c^{L} increases much more slowly than F_c^{Tr} with increasing B_ϕ and at $B_\phi=0.6$, F_c^{Tr} is nearly an order of magnitude larger than F_c^{L}. In addition to increasing with increasing B_ϕ, the ratio $F_c^{\mathrm{Tr}}/F_c^{\mathrm{L}}$ increases with decreasing B_ϕ as B_ϕ approaches zero due to

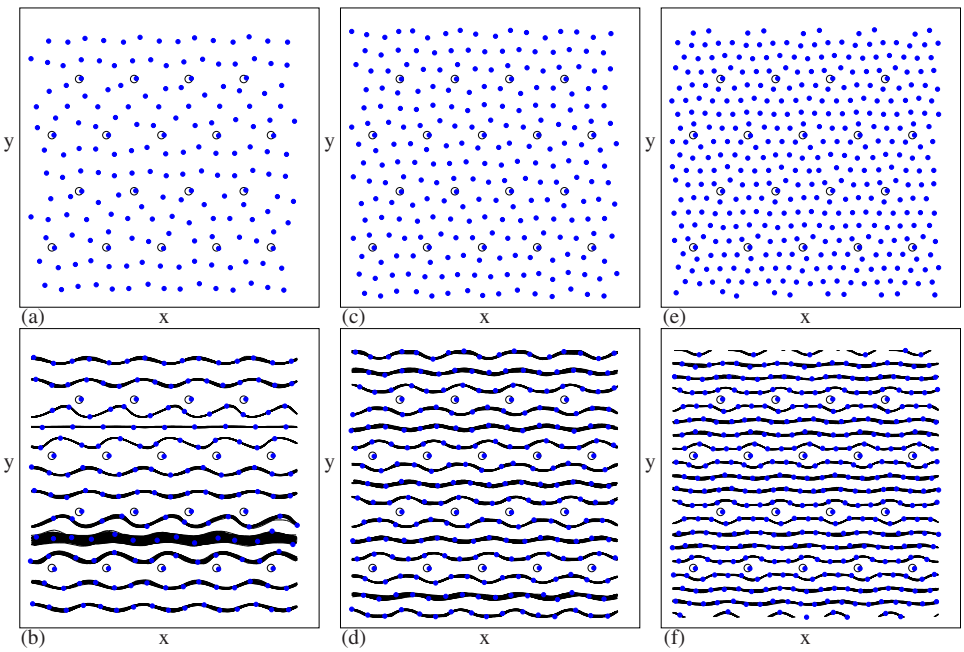

FIG. 3. (Color online) The vortex positions (black dots), pinning site locations (open circles), and vortex trajectories (black lines) for the system in Fig. 1(a). [(a),(b)] $B/B_\phi=8.0$, marked **a** in Fig. 1(b). [(c),(d)] $B/B_\phi=10.67$, marked **c** in Fig. 1(b). [(e),(f)] $B/B_\phi=17$, marked **e** in Fig. 1(b).

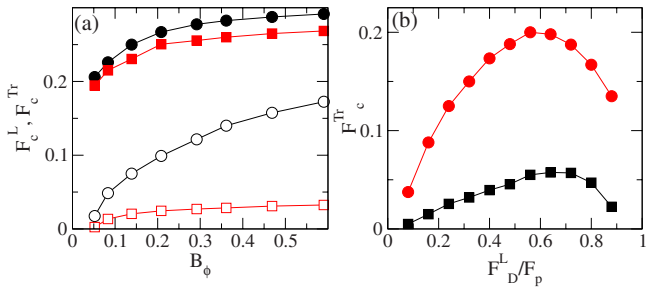

FIG. 4. (Color online) (a) The longitudinal critical depinning force F_c^{L} vs B_ϕ for $B/B_\phi=2.0$ (filled squares) and $B/B_\phi=2.5$ (open squares) and the transverse critical depinning force F_c^{Tr} vs B_ϕ for $B/B_\phi=2.0$ (filled circles) and $B/B_\phi=2.5$ (open circles) (b) F_c^{Tr} vs the applied longitudinal force F_D^{L}/F_p for $B/B_\phi=3.0$ (filled circles) and $B/B_\phi=3.67$ (filled squares).

the different rates at which the two thresholds approach zero.

The higher value of F_c^{Tr} compared to F_c^{L} can be understood by considering that longitudinal depinning occurs from the ground-state configurations of the interstitial vortices[2,3] and is determined by the repulsive interactions between the vortices at the pinning sites and the interstitial vortices. In the ground state, the interstitial vortices occupy positions that lower the repulsion from the pinned vortices, and the initial longitudinal depinning occurs when the interstitial vortices begin to move between the pinning sites, such as in Fig. 2(a). For the transverse depinning, when the interstitial vortices are moving at a sufficiently high velocity in the longitudinal direction they do not have time to slip between the pinned vortices in the transverse direction, but instead come into close proximity with the pinned vortices and interact strongly with them, resulting in a high repulsive barrier for depinning. If the longitudinal drive is set to a lower value before the transverse drive is applied, the interstitial vortices have more time to pass between the pinned vortices and F_c^{Tr} decreases. In Fig. 4(b) we illustrate this effect by plotting F_c^{Tr} versus F_D^{L}/F_p for $B/B_\phi=3.0$ and $B/B_\phi=3.67$. In both cases F_c^{Tr} increases from a low value with increasing F_D^{L}/F_p until reaching a maximum value at $F_D^{\mathrm{L}}/F_p=1.07$ for $B/B_\phi=3.0$ and at $F_D^{\mathrm{L}}/F_p=1.12$ for $B/B_\phi=3.67$. Above this drive, F_c^{Tr} decreases with increasing F_D^{L}/F_p as F_D^{L}/F_p approaches 1 since the vortices at the pinning sites begin to depin for the higher longitudinal drives, reducing the magnitude of the transverse critical current.

In summary, we have shown that a type of dynamical commensurability effect can occur for vortices in periodic pinning arrays. When interstitial vortices are moving between pinned vortices and an additional transverse force is applied, there is a finite transverse critical depinning force which oscillates with field. The oscillation is not simply related to the matching of the vortices with the number of pinning sites as in the case for the longitudinal depinning, but is associated with the dynamical structure of the vortices which allows for integer or noninteger numbers of rows of moving interstitial vortices between adjacent rows of pinning sites. The transverse commensurability effects are much broader than those seen for the longitudinal depinning, and each maximum in the transverse depinning force can span several matching fields. Remarkably, the transverse depinning force can be more than an order of magnitude larger than the longitudinal depinning force due to the fact that the moving interstitial vortices are unable to move between the pinned vortices without coming close to the pinned vortices, which creates a strong repulsive barrier for transverse depinning.

This work was carried out under the auspices of the NNSA of the U.S. DOE at LANL under Contract No. DE-AC52-06NA25396.

[1] A. T. Fiory *et al.*, Appl. Phys. Lett. **32**, 73 (1978); M. Baert *et al.*, Phys. Rev. Lett. **74**, 3269 (1995); U. Welp *et al.*, Phys. Rev. B **66**, 212507 (2002); V. Metlushko *et al.*, *ibid.* **59**, 603 (1999).
[2] K. Harada *et al.*, Science **274**, 1167 (1996).
[3] C. Reichhardt *et al.*, Phys. Rev. B **57**, 7937 (1998).
[4] G. R. Berdiyorov *et al.*, Phys. Rev. B **74**, 174512 (2006).
[5] D. J. Morgan and J. B. Ketterson, Phys. Rev. Lett. **80**, 3614 (1998); J. I. Martín *et al.*, *ibid.* **83**, 1022 (1999).
[6] E. Rosseel *et al.*, Phys. Rev. B **53**, R2983 (1996).
[7] C. Reichhardt *et al.*, Phys. Rev. Lett. **78**, 2648 (1997); C. Reichhardt *et al.*, Phys. Rev. B **64**, 014501 (2001).
[8] T. Giamarchi and P. Le Doussal, Phys. Rev. Lett. **76**, 3408 (1996); L. Balents *et al.*, Phys. Rev. B **57**, 7705 (1998).
[9] H. Fangohr *et al.*, Phys. Rev. B **63**, 064501 (2001); C. J. Olson and C. Reichhardt, *ibid.* **61**, R3811 (2000).
[10] A. M. Troyanovski *et al.*, Nature (London) **399**, 665 (1999); J. Lefebvre *et al.*, Phys. Rev. B **74**, 174509 (2006).
[11] J. Lefebvre *et al.*, Phys. Rev. B **78**, 134506 (2008).
[12] C. Reichhardt and F. Nori, Phys. Rev. Lett. **82**, 414 (1999).
[13] V. I. Marconi *et al.*, Phys. Rev. B **62**, 4096 (2000); G. Carneiro, *ibid.* **66**, 054523 (2002).
[14] P. T. Korda *et al.*, Phys. Rev. Lett. **89**, 128301 (2002).
[15] R. Besseling *et al.*, New J. Phys. **7**, 71 (2005).
[16] S. Anders *et al.*, Phys. Rev. B **62**, 15195 (2000).
[17] S. H. Brongersma *et al.*, Phys. Rev. Lett. **71**, 2319 (1993).
[18] C. C. de Souza Silva *et al.*, Phys. Rev. B **63**, 134526 (2001).
[19] G. Karapetrov *et al.*, Phys. Rev. Lett. **95**, 167002 (2005).